Unsteady Flowfield Behind a Vortex Generator Rapidly Pitched to Angle of Attack

Howard S. Littell* and John K. Eaton†
Stanford University, Stanford, California 94305

The unsteady flowfield resulting from sweeping a half-delta wing vortex generator partially embedded in a turbulent boundary layer from 0 to −18 deg angle of attack at a reduced frequency of 0.25 was probed with a cross-wire anemometer. Contour plots of vorticity and mean velocity as well as scalar descriptors of the flow such as circulation, peak vorticity, and vortex core location were calculated as a function of time for the formation and relaxation of the vortex. Some features of the unsteady development are accounted for by considering the effective angle of attack of the moving vortex generator and resulting motion of fluid shed by the leading edge.

Nomenclature

f = circular frequency of motion, Hz
k = reduced frequency Lf/U_{ref} [nondim]
L = chord of vortex generator, = 0.10 m
U = mean velocity in streamwise direction, m/s
U_e = local freestream velocity (local U_∞), m/s
U_{ref} = reference velocity, = 13.0 m/s
V_n = velocity normal to vane, m/s
X = distance down tunnel from boundary-layer trip, m
X' = distance along vane chord from pivot toward tip, m
X_{TE} = distance down tunnel from trailing edge of vane, m
α = physical angle of attack of vane, deg
α_e = effective angle of attack relative to shed fluid, deg
Γ = circulation circ/LU_e [nondim]
θ = time tU_e/X [nondim]
τ = time tU_{ref}/L [nondim]
ω = vorticity vort $\times L/U_e$ [nondim]

I. Introduction

THE maneuverability of a modern high-performance jet aircraft is often limited by flow separation over its control surfaces or by the overriding concern against stalling the engine inlet. Vortex generators have been used to delay separation in adverse pressure gradients for several decades but have a substantial drag pentalty. For this reason they are used only when absolutely necessary to prevent dangerous surprises or to extend the flight envelope. If boundary-layer control could be effected only when needed, a great deal of performance could be gained without the usual tradeoff of range or speed. An actuated vortex generator could provide such a measure of control, without the complexity and power drain of boundary-layer suction, for example.

A controlled vortex could also be useful to budget vortical fluid on a wing that is operating past its normal stall limit, if such a scheme could be shown to push off a growing separation region on demand. This would be useful in low-speed flight such as during a carrier landing or as a flight control in its own right. Tremendous moments could be created by selectively stalling part of a wing or fuselage under fly-by-wire control.

To utilize the control capability of an actuated vortex, it is imperative to investigate the unsteady flow resulting from the actuation process so as to be able to predict the effect on a boundary layer or a separated shear layer. This knowledge would also help guide the development of actuation strategy or perhaps the design of special vortex generators for specific purposes.

There has been considerable detailed work on vortex generator performance in steady flows ranging from the early work reported by Pearcey[1] to the recent work of Pauley and Eaton.[2] The only available experimental work on moving vortex generators was reported by Westphal and Mehta.[3] They oscillated a half-delta wing in the spanwise direction at constant angle of attack to investigate the effect of core wander on turbulence quantities. However, the motion was very slow, and so the flow could be considered quasisteady. Gad-el-Hak and Ho[4,5] have examined the flow downstream of a pitching delta wing in uniform flow, which is quite different from the vortex generator embedded in a boundary layer. One major difference is the fact that slow boundary-layer fluid is rolled up in the wake of the vortex generator while the delta wing produces an accelerated core flow that is subject to bursting.

This study had three primary objectives: 1) to identify any large-scale structures developed during the vortex generator actuation, 2) to determine the time of initial shedding of a longitudinal vortex, and 3) to measure the propagation velocity of the unsteady structure. These goals all relate to the eventual application of actuated vortex generators to flow control systems. Variation of the system parameters was unfortunately not a reasonable objective in view of the large amount of time required to acquire and analyze the data from a single case. It is felt that the observed behavior is representative of cases where a vortex generator is actuated rapidly to small angles of attack.

II. Experimental Apparatus and Techniques

The wind tunnel used for this investigation is a 61 × 13 cm nominally zero pressure gradient facility described by Pauley and Eaton.[2] The tunnel is of open circuit design and has a freestream turbulence level of 0.3% at a reference velocity U_{ref} of 13 m/s. The test surface is one of the 61 cm walls. The boundary layer on this wall is tripped shortly downstream of the contraction exit. The available test section is 2 m in length downstream of the boundary-layer trip.

As shown in Fig. 1, the vortex generator was installed on the test wall at a location 54 cm downstream of the trip where the undisturbed boundary layer was approximately 1.5 cm thick with a momentum thickness Reynolds number of 1150. The vortex generator was a 22 deg included angle half-delta wing with a chord of 10 cm and a height of 4 cm; therefore the generator was only partially embedded in the boundary layer as is

Received Sept. 5, 1989; revision received March 12, 1990.

*Research Assistant, Department of Mechanical Engineering. Member AIAA.
†Associate Professor, Department of Mechanical Engineering. Member AIAA.

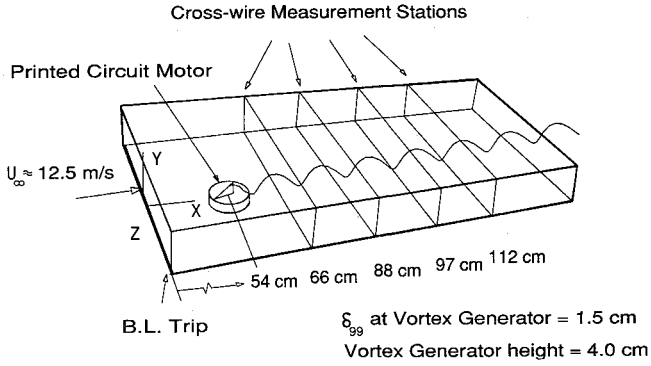

Fig. 1 Wind tunnel schematic.

typical in aeronautical applications. It was constructed of 1/32 in. aluminum with square edges. This vane had a tab below its centroid clamped with a setscrew in a 3/8 in. diameter shaft that was sealed in the wall against leakage by foam rubber. The end of this shaft was flush with the test surface so that no protrusion other than the vane disturbed the boundary layer. The shaft was connected directly to a Precision Motion Industries printed circuit motor powered by a servo amplifier. The servo system was controlled by the digital-to-analog converter in the Masscomp MC5400 data acquisition/control computer. Vane position was obtained using a rotary variable differential transformer (RVDT), which also supplied position for the feedback loop of the controller. The control input for the present study was a step voltage that produced the desired angle of attack under steady-state conditions.

A crosswire anemometer was used to probe the flow at four locations downstream from the vortex generator. A slot in the opposite wall of the tunnel at each of these locations allowed a computer-controlled two-dimensional traverse to move in the Z direction as well as the Y direction. The traverse is equipped so that the crosswire may be rotated around its axis so that all three components of velocity may be measured in a steady or in a periodic flow with a known phase reference as is the case here. The hotwires were connected to a pair of Precision Measurement Engineering (PME) Constant Temperature Anemometer bridges, low-pass filtered at 20 kHz, then amplified using a PME buck and gain. The signals were clamped using the Masscomp sample-and-hold running at the sampling frequency to ensure simultaneous velocity readings for the two hotwires, then read using the analog-to-digital converter. The calibration procedure used for the crosswire was essentially the same as described in Anderson and Eaton.[6] Only ensemble-averaged mean quantities were used in this study, and the uncertainty of each as reported in Ref. 6 was 3% of the local U.

The data were stored as raw digital values along with a calibration file for subsequent reduction. A typical acquisition procedure involved taking a Y profile at a given Z location in two steps. The crosswire would first be positioned to measure UV velocities and the complete profile taken with 100 ensembles at each Y location. The crosswire was then rotated to measure UW velocities and the profile repeated. The traverse would then move to the next Z location and repeat the process. A typical plane of data would consist of several dozen spatial locations, each with two wires in two orientations, with 200 samples of each for 100 ensembles. This large amount of data was viewed using a Silicon Graphics IRIS workstation using a graphics processor developed at NASA Ames called TURB3D.

The data sets that will be presented here are from the four measurement stations shown in Fig. 1. The grid for the points at the 66-cm plane was evenly spaced at 0.5 cm intervals while points of the subsequent planes were spaced at 1.0 cm. The vortex behaves as a potential vortex close to a boundary and translates across the wall as it moves in the downstream direction, so the latter planes were of necessity wider in the Z direction. The acquisition frequency for the 66-cm plane was 2500 Hz, and subsequent planes were probed at 1500 Hz. At the 66-cm station, 50 ensembles were taken whereas at the coarser grid locations downstream 100 ensembles were run. The Masscomp computer was used to control the tunnel, actuate the vane, and acquire the data so the data were automatically phase locked to the actuation.

The three components of measured velocities were interpolated to a fine grid using an alternating bidirectional cubic spline scheme. One-dimensional splines were fit between each measured grid point velocity in the Z direction, then more splines were fit in the Y direction at the desired spacing. The Y splines were then evaluated for the desired intermediate points and averaged with the values obtained from fitting the Y direction first and then the Z direction. The interpolation spacing was chosen so as to preserve the original data unchanged, and this procedure did not smooth the data at all. Streamwise vorticity was computed by fitting cubic splines to the measured and interpolated velocities in a plane and evaluating the necessary derivatives analytically from the spline. Circulation was defined as the integral of all vorticity greater than 5% of the peak. The uncertainty in this method's resolution of peak vorticity and circulation was 5 and 1%, respectively, for 0.5-cm grid spacing, as found by applying the entire procedure to discretely sampled analytic data from an Oseen vortex.[7] The uncertainty of the streamwise vorticity was calculated considering the uncertainty in the secondary velocity measurements and probe positioning errors as $\omega_{unc} = 1.3$ (nondimensional) and $\Gamma_{unc} = 0.00148$. These estimates are conservative since the potential measurement errors are not independent from point to point, and the vorticity calculation involves differences of measured velocities. Accounting only for statistical variations due to the finite number of ensembles, the uncertainties are $\omega_{unc} = 1.1$ or 7.8% of the peak vorticity and $\Gamma_{unc} = 0.000792$ for $\Gamma = 0.0250$ (3.2%). These were based on small samples of a turbulent phenomenon but are probably a better indication of the true uncertainty of the calculations than independent uncertainties for each point. We therefore estimate the total uncertainty for the peak vorticity at steady state would be less than 10% and for circulation less than 4%. We believe these uncertainties do not obscure the reported trends enough to limit their usefulness.

Computation of spanwise (Z) and normal (Y) vorticity components was more difficult because of the relatively wide streamwise spacing of the data. To evaluate these components it was assumed that temporal features of the flow were just convected downstream and changed slowly with X. This is essentially Taylor's hypothesis applied to a coherent structure instead of a small eddy. The X displacements of consecutive time steps were calculated using the instantaneous local streamwise velocity. Therefore the uniform grid in Y and Z was available, but the transformed spacing in X was nonuniform. This guided the selection of sampling rates so as to obtain a similar spacing in X as was available in the other directions. A spline was then fit to several points "upstream" and "downstream" to obtain X derivatives, thus allowing Y and Z vorticities to be computed. These vorticity values were only used qualitatively so the uncertainty inherent in this application of Taylor's hypothesis, though undoubtedly large, was not seen as limiting the usefulness of the results.

III. Results

The input to the printed circuit motor controller was a step increase in voltage that produced the desired angle of attack at steady state. The vane was initially at zero incidence and was flipped to -18 deg. This corresponds to the tip of the vane moving in the positive Z direction resulting in a vortex of positive circulation that will translate in the negative Z direction owing to its image in the test surface. The vane's motion is completed in a nondimensional time $\tau \approx 2$, which corresponds to twice the time it takes a fluid particle at the reference velocity to move the length of the generator.

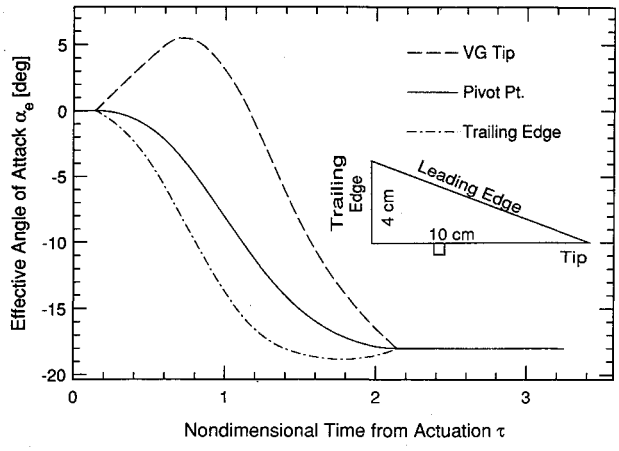

Fig. 2 Vortex generator angle and effective angle of attack due to motion.

Since the vane is operating in a finite velocity flowfield, its effective angle of attack is a function of its pitch rate as well as its instantaneous physical orientation. The velocity normal to the vane at any point along the length of the vane is

$$V_n = -U\sin(\alpha) + \dot{\alpha}X'$$

where α is the instantaneous angle of attack, $\dot{\alpha}$ is the pitch rate, and X' is the distance from the center of rotation. We can then define an effective angle of attack α_e as

$$\sin(\alpha_e) = -V_n/U$$

The response of the vane actuation system is shown as the pivot point trace in Fig. 2, along with the effective angle of the tip and the trailing edge. As can be seen on the plot at a given actuation time, there is a wide range of incidence angles along the vane.

In physical terms the vane tip is initially outrunning the freestream flow, and thus its effective angle of attack is positive, even though the stiff vane is actually at a negative angle of attack. Just as the tip is outrunning the flow, the trailing edge is being pushed into the freestream so that it appears to be at an angle of attack greater (more negative) than the vane due to its motion. Intermediate points along the chord or the leading edge have effective angles that lie between that of the pivot point and the appropriate end of the vane. The manifestation of this effect would be a progression of the separation region from the trailing edge toward the tip. This propagation was observed using flow visualization on a complete delta wing by Gad-el-Hak and Ho.[4] A plot similar to Fig. 2 may be computed for their flow with the more exaggerated behavior occurring at the trailing edge since their delta wing was from 0–30 deg, and this sweep took place in $\tau = \pi/2$ whereas that of the present study took $\tau \approx 2$. This yields substantially higher angular velocity for the delta wing, so the overshoot of the trailing edge is more pronounced than that of the vortex generator. Gad-el-Hak also reported that there was no propagation phenomenon on the 30–0 deg sweep, again pointing to the complex nature of this type of flowfield.

Unfortunately, it is impossible to predict the path of any fluid that for instance passed near the tip of the vortex generator early in its motion and thus had X vorticity that is negative. It must be recognized that some of the fluid that is rolled into the vortex will have had its origin very close to the wall and will have a low total pressure from previous viscous interaction (see Dunham[8]). This presumably accounts for the velocity deficit that is always observed for a wall vortex. The situation would be further complicated by the fact that the vane actually performs work on nearby fluid while it is in motion, thereby modifying the total pressure again.

Table 1 Values associated with contour lines

Quantity	Description	Initial contour	Subsequent contours
Velocity	Heavy solid	0.99 U/U_e	——
	Solid	0.95 U/U_e	−0.05 incr.
	Dashed	1.05 U/U_e	0.05 incr.
Vorticity	Solid	1.5	1.5 incr.
	Dashed	−1.5	−1.5 incr.

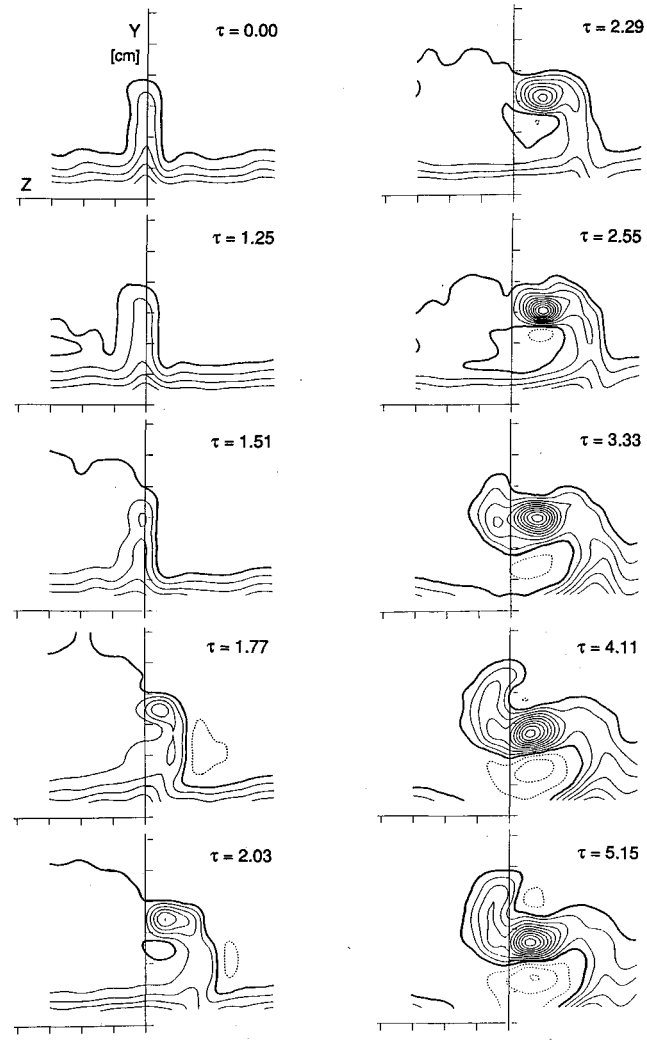

Fig. 3 Formation streamwise velocity contours vs nondimensional time at 66 cm (see Table 1).

Formation of Vortex

The presentation of the entire data set is impossible without the aid of a three-dimensional graphics workstation. The measurements are presented here as planes of data at selected time steps that are representative of the trends of the development. The data presented are normalized by the local freestream velocity that varied nearly linearly from 12.51 m/s at the first measurement station to 12.93 m/s at the last station.

Figures 3 and 4 show the streamwise velocity and streamwise vorticity contours for the 66-cm station. The maximum and minimum vorticity and the positive circulation are plotted as a function of time in Fig. 5. The initial state of the boundary layer and wake of the vane can be seen in the $\tau = 0.00$ frame of Fig. 3. The slight bumpiness of the boundary layer is a characteristic of the tunnel and is also documented in Pauley and Eaton[2] and Eibeck and Eaton.[9] The wake of the vane is symmetric about the Y axis, and its height is still approximately equal to the vane height of 4 cm. In Figs. 3 and 4, the first sign of the vane actuation is the asymmetry of the velocity contours at $\tau = 1.25$, followed by the appearance of the trail-

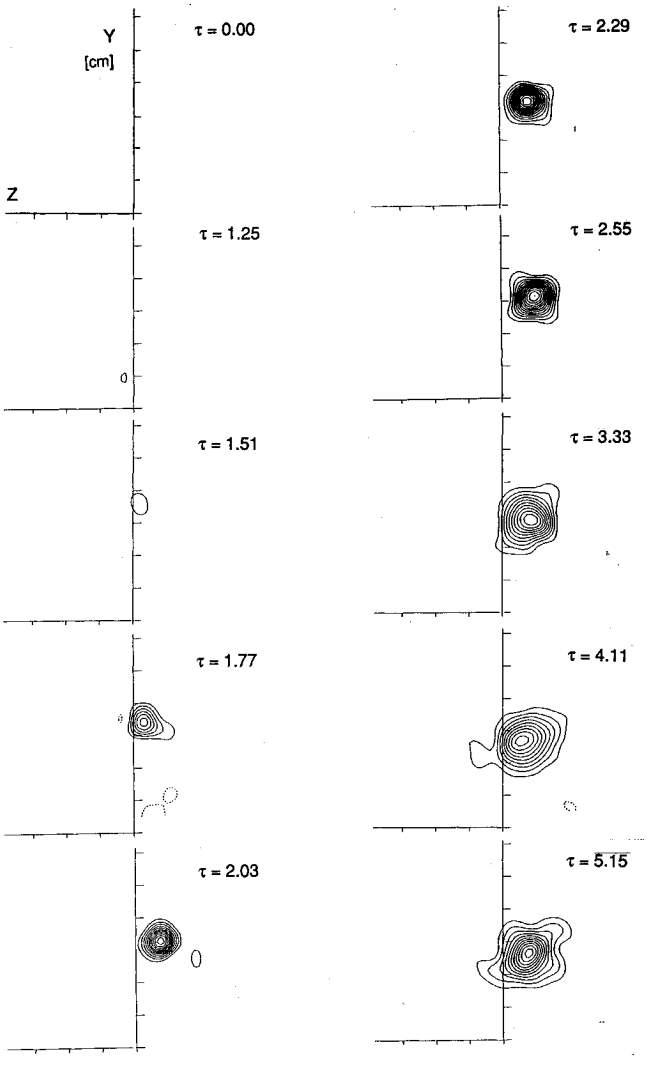

Fig. 4 Formation streamwise vorticity contours vs nondimensional time at 66 cm (see Table 1).

ing vortex about 3.7 cm away from the wall at $\tau = 1.51$. As time progresses the vortex continues to roll up, and for a while there is a region of higher than freestream velocity fluid on the $-Z$ side of the vortex, as in $\tau = 1.77$ and 2.03. At about the same time, there is a packet of fluid deep in the boundary layer directly below the vortex that has negative X vorticity. The primary vortex continues to roll up and increases steadily in circulation until it asymptotes after $\tau \approx 4.0$. The peak vorticity, though, is not monotonic and appears to drop after $\tau \approx 2.55$. The upper section of the vane wake reappears at about this time and becomes stronger as time goes on. There also appear nodes of high velocity fluid above and below the vortex, probably due to the centrifugal lowering of the pressure just as in the accelerated core of a free vortex. Figure 6 shows the Y and Z location of the peak vorticity and the minimum axial velocity at the 66-cm station.

Figure 7 shows time records of the Y vorticity at a height of 2 cm above the wall. The time axis is scaled so that $\Delta X = U_e \Delta t$. Of particular note is the structure at $\tau = 1.74$ in the 66-cm plot that appears to be a concentrated packet of Y vorticity of negative sign. This structure may be traced to succeeding planes and appears to roughly retain its form, even though its intensity decreases significantly. This is probably the record of passage of a classic startup vortex shed by the vane as it started to lift. In a vortex, one expects to find circular or spiraling streamlines; to check this, the data were again transformed into a physical grid using the aforementioned procedure. Using a reference frame moving at 93% of freestream velocity allowed details to be seen that would otherwise be washed out

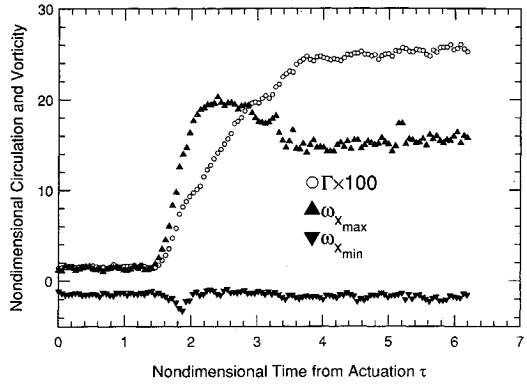

Fig. 5 Formation peak vorticity and circulation vs nondimensional time at 66 cm.

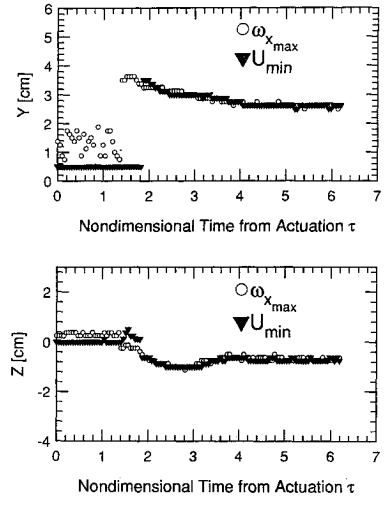

Fig. 6 Formation core location vs nondimensional time at 66 cm.

by the mean flow. The instantaneous streamlines were traced using the capability of the program TURB3D and indeed spiraled only in the highly vortical region discussed above. The nature of this three-dimensional structure is readily apparent when rotated in real time using the graphic workstation, but a single plot of it is very difficult to appreciate. The streamlines describe a straight vortex almost normal to the wall but tilted slightly "downstream." This is to say that portions of the vortex higher away from the wall crossed the measurement plane first, followed by the portions closer to the wall. This structure was the only wall normal vortex found in this data set and is still identifiable though somewhat harder to pick out using other reference frames or transformations. The same technique was applied to the other measurement locations, but due to the coarseness of the grids and perhaps diffusion of the structure it was more difficult to detect, though still possible in the 81- and 97-cm data sets.

Using the times of passage of the starting vortex from Fig. 7 and the distances from the vane, it was possible to compute an effective propagation velocity of the structure. These data appear as Fig. 8, and as shown, a least squares fit to the data yields a velocity of approximately 90% of the reference freestream velocity of 13.0 m/s.

Planes of the ZY data that appeared to mark similar stages of the unsteady process are reproduced in Figs. 9 and 10. The related planes in Figs. 3 and 4 are $\tau = 1.77$, $\tau = 2.29$, and $\tau = 5.15$. These planes were chosen on the basis of time axis plots such as Fig. 7. The convection times were accounted for by selecting times for which the value of θ (tU_e/X) was the same at each station. These plots suggest that the train of events shown in more detail for the 66-cm station continue to retain their identity and temporal spacing further downstream. The data for the downstream station were spaced at 1 cm, and

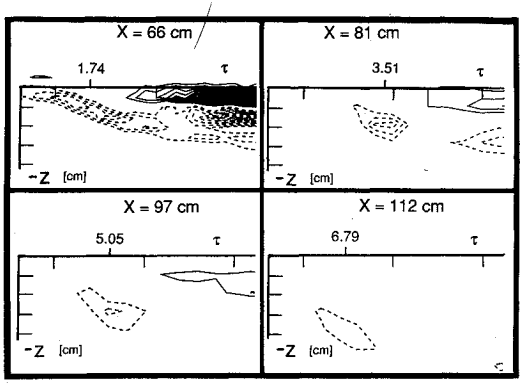

Fig. 7 Formation wall normal vorticity vs time for each measurement location showing starting structure.

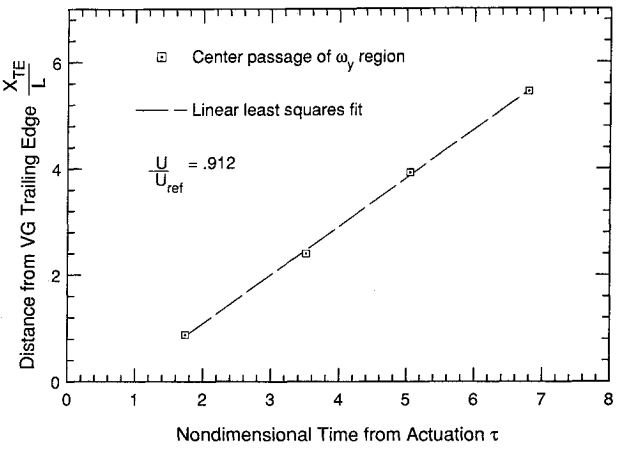

Fig. 8 Location of starting structure vs nondimensional time.

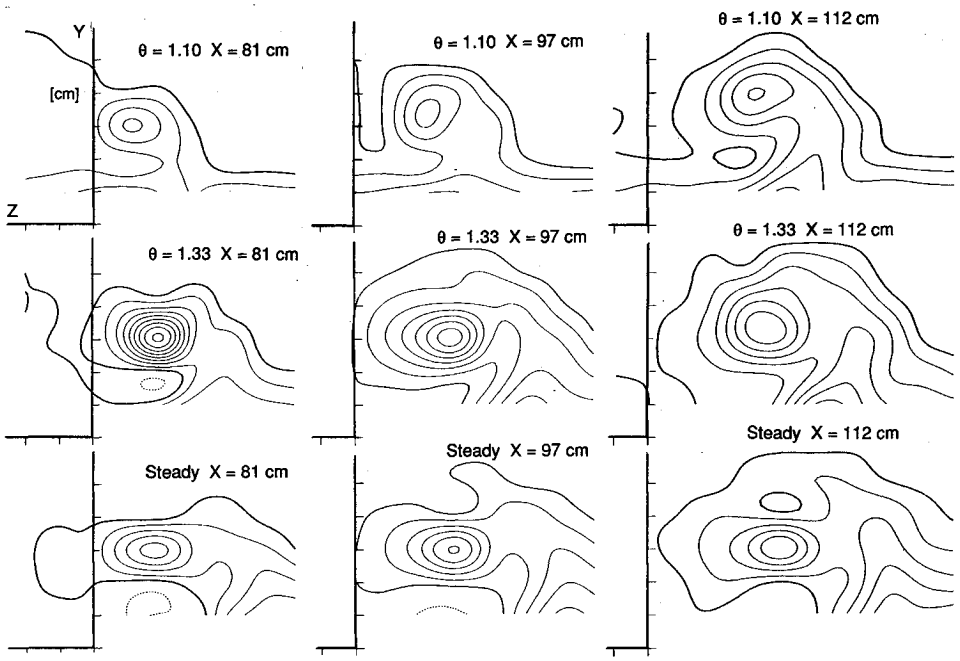

Fig. 9 Streamwise development of contours of velocity (see Table 1).

although resolution was sufficient to capture overall behavior, it was not capable of resolving fine details such as the peak vorticity. The circulation stayed almost constant in the streamwise direction as noted by many previous researchers, and by taking a very fine grid of steady-state data, it was found that the peak vorticity decreased slowly in the streamwise direction at steady state as shown in previous studies.

One notable difference between the downstream locations and the 66-cm station is the full rollup of the wake as can be seen by comparison of the steady-state plots. In a study performed by Mehta and Cantwell,[10] it was found that the generator wake rolls up in approximately three generator heights downstream from the trailing edge of the vane. Their vortex generator was much taller than the boundary-layer thickness, so minimal interaction was present. For the present study, the first measurement station was 2.22 vane heights behind the trailing edge of the generator, and the second was 6.03 vane heights behind the trailing edge. The first station shows the vane wake strongly in the velocity plot, Fig. 3, but gives a less exaggerated shape in the vorticity plot, Fig. 4. The velocity record of the wake is almost completely gone by the 81-cm station, and the vorticity contours have taken a rounded triangular shape that they keep from then on. This corresponds to the behavior noted by Mehta and Cantwell, even though their vortex was not embedded in the boundary layer.

Relaxation of Vortex

As can be surmised from Figs. 3–6, the vortex has reached a steady state at 66 cm for $\tau > 5.0$, and at $\tau = 6.24$ the vane was flipped back to an angle of attack of 0 deg. Note that relaxation times τ are referenced to the beginning of the relaxing sweep of the vane. Data were recorded for this case only at the 66-cm station. Again, the effective angle of attack during the motion is an important concept. This can be described much the same as Fig. 2 inverted; that is, the tip overshoots the steady angle of attack of -18 deg and goes on to exceed -24 deg before falling quickly to zero. Near the end of the motion, the trailing edge overshoots 0 deg slightly as it did -18 deg in Fig. 2. This is somewhat misleading, since there exists a complex three-dimensional flow around the vane when it begins to return to 0 deg, which was not present on the 0 to -18 deg sweep. It may be assumed that the flow on the suction side of the vane is following the vane itself near the trailing edge under the main vortex; therefore the rear portion of the leading edge would begin shedding negative vorticity sooner after actuation than an inverted Fig. 2 would suggest.

The first perceptible deviation from steady state is shown in the first time step in Figs. 11 and 12, $\tau = 1.04$, and amounts to a weakening of the velocity deficit in the vortex generator wake. As can be seen in Fig. 13, the circulation in the vortex goes up slightly and then begins a steady drop. This is not

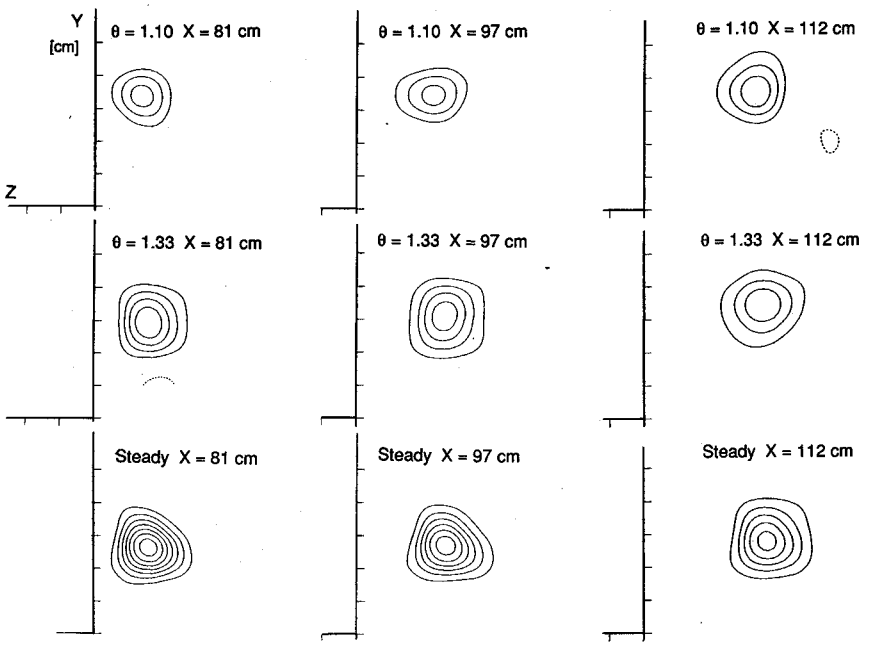

Fig. 10 Streamwise development of contours of vorticity (see Table 1).

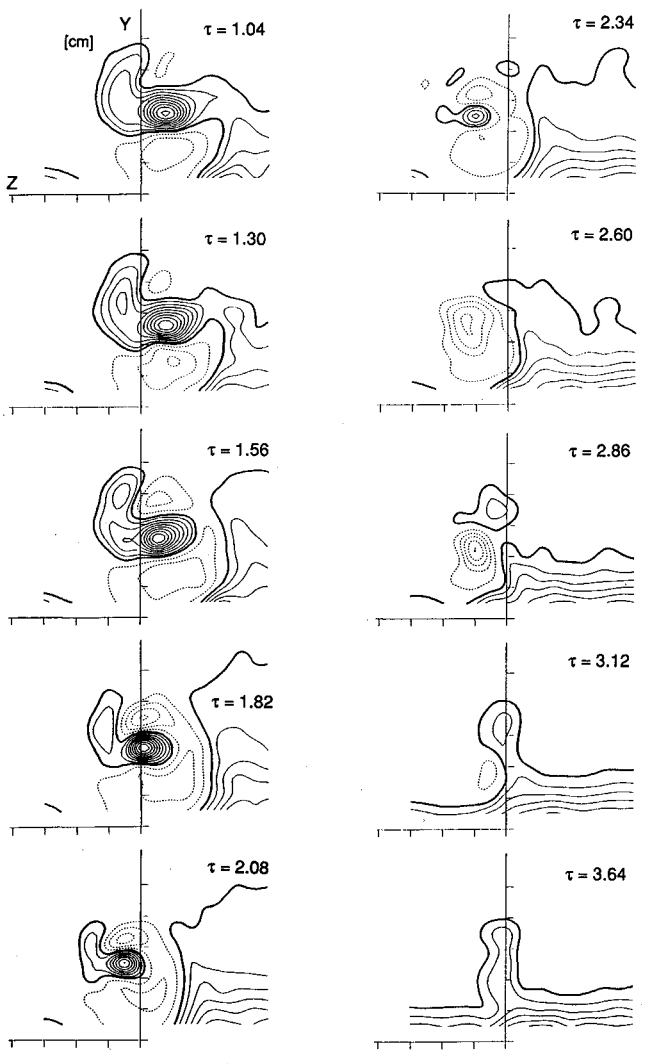

Fig. 11 Relaxation streamwise velocity contours vs nondimensional time at 66 cm (see Table 1).

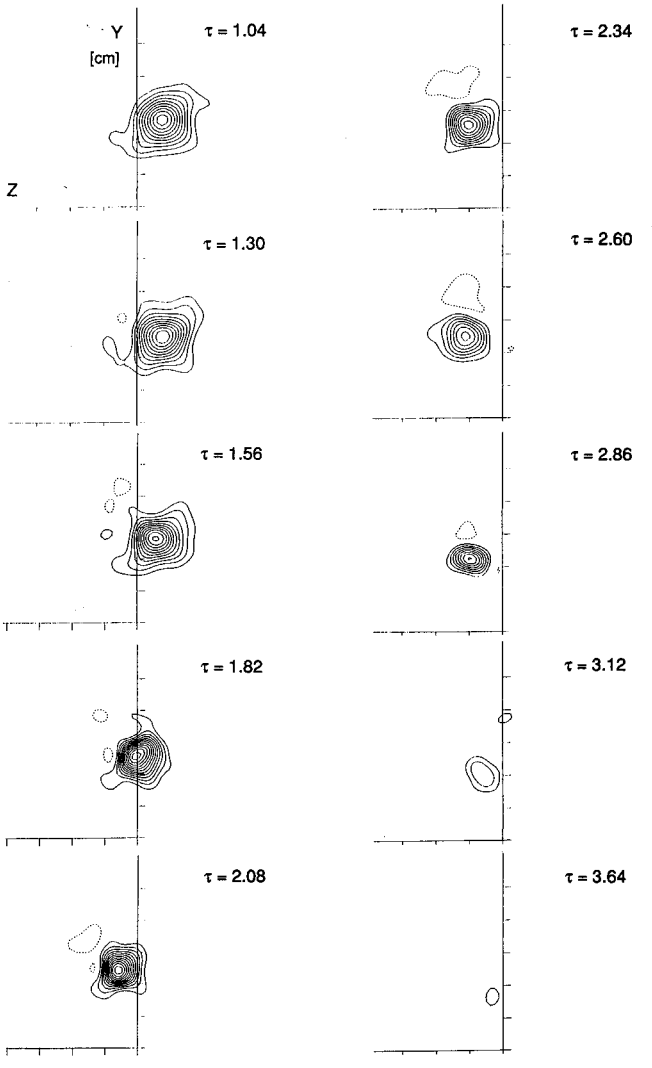

Fig. 12 Relaxation streamwise vorticity contours vs nondimensional time at 66 cm (see Table 1).

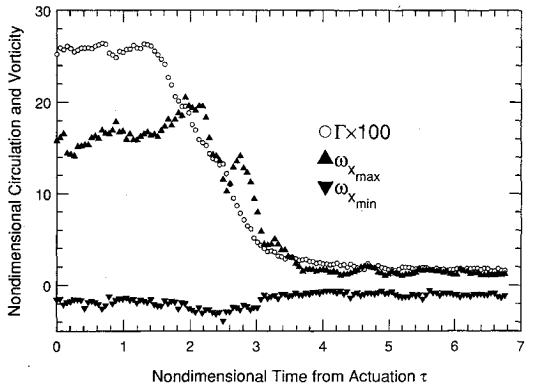

Fig. 13 Relaxation peak vorticity and circulation vs nondimensional time at 66 cm.

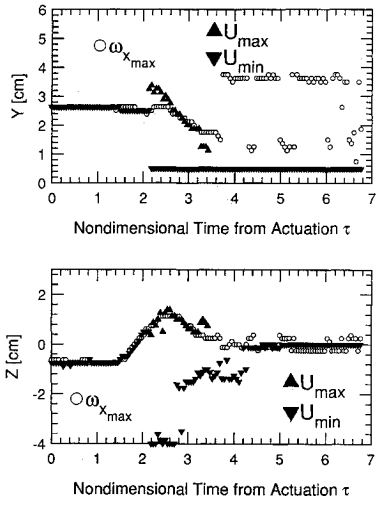

Fig. 14 Relaxation core location vs nondimensional time at 66 cm.

readily apparent in Fig. 12. What the contour plots do show are relatively long-lived regions of negative vorticity. These also show up as a depression in the minimum X vorticity in Fig. 13. The vortex continues to grow weaker in circulation even though the peak vorticity actually climbs for several time steps centered around $\tau = 2.0$. The peak falls until $\tau = 2.75$ where it again swings up and then once again falls.

After $\tau = 1.04$ the wake begins to shrink and grow weaker while the vortex core moves around quite markedly; its path can be seen in Fig. 14. These plots show that the vortex remains at a steady height above the wall before $\tau \approx 2.6$ but moves to the other side of the tunnel centerline. One very interesting effect occurred between $\tau = 2.34$ and $\tau = 2.60$; the typically observed velocity deficit in the core of the boundary-layer vortex quickly changes to resemble a free vortex with an accelerated core. For this reason, the location of the maximum velocity was also plotted on Fig. 14, though the interpretation of these requires reference to Fig. 11 and 12. The first few points plotted for the maximum velocity appear as accelerated regions above the vortex, whereas at $\tau = 2.76$ the Y and the Z traces coincide with the vortex core. This continues until $\tau = 3.2$, after which the vortex is fading rapidly.

It seems reasonable to look for a stopping structure in the form of a packet of Y vorticity of positive sign, but no coherent vortex was found. This would represent the release of the vorticity bound to the lifting vortex generator. There was a somewhat elongated region of Y vorticity as seen in Fig. 7, but a concerted effort at streamline identification yielded no spiraling.

A comparison of the behavior of the vortex circulation is given as Fig. 15. The relaxation process has been inverted so that the paths of the rise and fall overlap, allowing easy comparison. It may be seen that the vortex starts its collapse at nearly the same rate and at exactly the same time as the formation process. Toward the end, the relaxation falls off quickly, while the formation process approaches its final level more gradually. This may be explained as the accelerated core present at the end of the relaxation washing out more quickly than the decelerated core can build up circulation in the formation process.

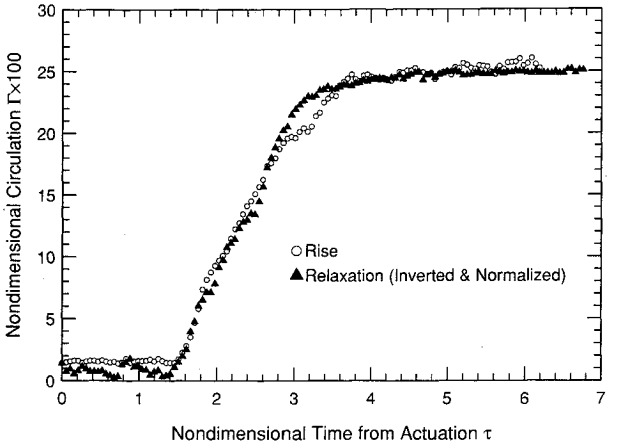

Fig. 15 Comparison of formation to relaxation circulation development at 66 cm.

IV. Discussion

The present measurements provide a fairly complete picture of the unsteady development of the flow downstream of an actuated vortex generator. The causes of some of the observed features are not clear because we lack information on the details of the flow in the immediate vicinity of the vane itself. This type of analysis could be better facilitated by an unsteady tracing of streaklines in the neighborhood of the vane leading and trailing edges.

The primary objective motivating this study was the description of the downstream behavior of the flowfield resulting from pitching a vortex generator rapidly to angle of attack. One interesting feature was the presence of a rolled-up starting vortex, and although not a dominant feature, it was clearly measurable and useful to trace as a precursor to the appearance of the streamwise vortex. The streamwise vortex was seen to build up quickly in relation to the time the vane was in motion. The relaxation of the vortex was seen not to be preceded by a rolled-up stopping vortex but exhibited a much greater spanwise core movement than the formation. This core motion was pronounced enough to warrant special attention in the design of a practical device, as it may trigger changes in a boundary layer close to separation. During the relaxation, the strong velocity deficit in the core was replaced by an accelerated core, signalling a major change in the nature of the vortex.

The delay from the onset of motion to the shedding of the longitudinal vortex is critical for the practical application of an actuated vane, and by comparison of Figs. 2 and 5 it is easily determined that the vortex arrives at the first measurement location before the vane even finishes its motion. If it is assumed the vortex convects at 90% of U_e, the flight time of the vortex from the trailing edge of the generator was $\tau = 1.0$. This puts the passage of the vortex past the trailing edge at $\alpha \approx -1$ deg.

Another important parameter of this phenomenon is the speed at which the vortex convects downstream once clear of the vane's influence; this was shown to be over 90% of the free-stream velocity by tracing the flight of the starting vortex. It was also determined that distinctive stages of the formation maintained their temporal spacing as they moved downstream.

Some interesting features of this flow can be attributed to the motion of the vane giving rise to an effective angle of attack that varies along the vane. In Fig. 2 it was shown that the earliest positive X vorticity is shed from the corner of the lead-

ing edge nearest the trailing edge, so it would be expected that the vortex would first appear far from the wall and subsequently move towards it. This is shown to be the case in Fig. 6. Also using Fig. 2, it was shown that negative vorticity could be produced by the motion of the vane, and it is tempting to attribute the region of negative vorticity in Fig. 4 at $\tau = 1.77$ to this cause. The overshoot in peak X vorticity seen in Fig. 5 may be viewed as the result of the trailing edge overshoot during actuation. Unfortunately, this is not entirely satisfactory for formation, since the peak X vorticity invariably occurs in the core of the vortex, where the fluid's origin is near the forward tip of the leading-edge separation. This leads us to believe the peak in Fig. 5 is unlikely to be a product of the overshooting trailing edge, but no plausible explanation presents itself.

An important observation that can be made from any of Figs. 3–6 is simply that the unsteady process is complete in the time in which the vane is in motion plus the (presumed) constant convection time past the vane of the fluid that bears the vortex. The actuation time is $\tau = 2.0$, and the convection time of fluid such as the startup structure would be $\tau \approx 1.09$, for a total of $\tau \approx 3.1$. As shown in Fig. 5, the first sign of the vortex apepars at $\tau \approx 1.4$, and by $\tau \approx 4.5$ the vortex statistics and position are constant. The reduced frequency of this flow is not large, $k = 0.25$ using back-to-back formation and relaxation to obtain the frequency, which is probably higher than a practical device used to control separation could attain. It is then plausible to expect the full benefit of a vortex-boundary layer interaction on demand, allowing for convection time based on a velocity between 90 and 95% of U_e.

The peak X vorticity during the relaxation experiences two upswings near $\tau = 2.0$ and $\tau = 2.8$. The first upswing is likely due to the strongly overshooting tip during the early relaxation motion. The second upswing in X vorticity is tied up with the sudden acceleration of the core seen at $\tau = 2.6$, but in a manner that is clouded by other possible effects. It is also probable that the long-lived negative vorticity trail seen in Fig. 12 during the relaxation is the result of the complicated shedding of negative vorticity from portions of the vane near the trailing edge. The position of the negative vorticity is somewhat suspect, being on top of the vortex instead of beside it, until it is realized that the secondary flowfield is still much as one would expect for the steady vortex. In this system there are tangential velocities in this negative vorticity region of $0.25U_e$ that would tend to wrap the negative vorticity around the main vortex. The effective angle of attack moves the separation region shedding positive vorticity down the leading edge toward the tip. This early release of the feeder sheet and vortex puts it farther in the $+Z$ direction than if released farther down the chord, just as if it had been formed by a shorter vortex generator. This is a possible cause of the strong core movement seen in Fig. 14, along with the weak induced velocity due to the negative vorticity. The timing of the movement gives further weight to this argument because, as shown in Fig. 12, the Z motion starts at the same time as the appearance of the negative vorticity.

The timing of the vane motion during relaxation is similar to that of the formation process, and as can be seen in Figs. 11–14, the entire process is complete in $\tau \approx 3.1$.

One interesting event that is only hinted at by this data set must occur somewhere downstream of the 66-cm station during relaxation. The accelerated core is spatially situated so as to run into the original velocity deficit at some downstream location. This may occur as a vortex burst, with a sudden deceleration and rise in core pressure, or since the slow core in front must also be at a low static pressure due to its circulation, the faster core might instead pierce the slow region without breakdown. Another possibility is that the two regions have sufficiently different induced velocity so that they translate in the Z direction at a different rate and the high-speed region passes to the side of the lower-speed region. Since the downstream data taken here do not include relaxation, we can only speculate as to what may occur.

In summary, it was shown that there exists definite nonmonotonic behavior in both the formation and relaxation of the vortex. The formation includes the appearance of a starting vortex and some wall-normal core motion. The relaxation did not produce a rolled-up stopping vortex but did exhibit strong spanwise core motion and a long-lived trail of opposite-signed longitudinal vorticity above the main vortex.

V. Conclusions

The unsteady flow produced by an actuated vortex generator partially embedded in a turbulent boundary layer has been investigated using a crosswire anemometer. A startup structure in the form of the classical starting vortex has been identified and traced in its downstream flight. The velocity of this vortex was found to be constant and greater than 90% of freestream velocity. The entire unsteady behavior of the formation and relaxation of the vortex was confined to a time approximately equal to the actuation time of the vortex generator plus the convection time past the generator chord.

Some well-established features of the unsteady flowfield were accounted for by a theorized effective angle of attack due to the motion of the vortex generator. Some facets of the flow do not readily lend themselves to an explanation, such as a sudden acceleration of the normally retarded vortex core during the unsteady relaxation of the vortex. Very precise flow visualization would probably shed light on the actual processes involved in this highly three-dimensional, unsteady turbulent flow.

Acknowledgments

This project was supported by the Air Force Office of Scientific Research under contract F49620-86-K0020. The authors would also like to thank the Center for Turbulence Research for the use of the IRIS workstation.

References

[1]Pearcey, H. H., "Shock-Induced Separation and Its Prevention by Design and Boundary Layer Control," *Boundary Layer and Flow Control,* Vol. 2, edited by G. V. Lachmann, Pergamon, Oxford, England, 1961.

[2]Pauley, W. R., and Eaton, J. K., "The Fluid Dynamics and Heat Transfer Effects of Streamwise Vortices Embedded in a Turbulent Boundary Layer," Thermosciences Div., Dept. of Mechanical Engineering, Stanford Univ., Stanford, CA, Rept. MD-51, 1988.

[3]Westphal, R. V., and Mehta, R. D., "Interaction of an Oscillating Vortex With a Turbulent Boundary Layer," *Experiments in Fluids,* Vol. 7, No. 6, 1989, pp. 405–411.

[4]Gad-el-Hak, M., and Ho, C. M., "The Pitching Delta Wing," *AIAA Journal,* Vol. 23, No. 11, Nov. 1985, pp. 1660–1665.

[5]Gad-el-Hak, M., and Ho, C. M., "Unsteady Vortical Flow Around Three-Dimensional Lifting Surfaces," *AIAA Journal,* Vol. 24, No. 5, May 1986, pp. 713–721.

[6]Anderson, S. D., and Eaton, J. K., "An Experimental Investigation of Pressure Driven Three-Dimensional Turbulent Boundary Layers," *Journal of Fluid Mechanics,* Vol. 202, 1989, pp. 263–294.

[7]White, F. M., *Viscous Fluid Flow,* McGraw-Hill, New York, 1974, p. 237.

[8]Dunham, J., "The Static Pressure in a Vortex Core," *Aeronautical Journal,* Vol. 83, No. 826, Oct. 1979, pp. 402–406.

[9]Eibeck, P. A., and Eaton, J. K., "An Experimental Investigation of the Heat Transfer Effects of a Longitudinal Vortex Embedded in a Turbulent Boundary Layer," Thermosciences Div., Dept. of Mechanical Engineering, Stanford Univ., Stanford, CA, Rept. MD-48, 1985.

[10]Mehta, R. D., and Cantwell, E. R., "Properties of a Half-Delta Wing Vortex," *Fluid Dynamics Research,* Vol. 4, No. 2, 1988, pp. 123–137.